Long-wavelength interface modes in semiconductor layer structures

M. Schubert,[1,*] T. Hofmann,[1] and Jan Šik[2]
[1]*Institute of Experimental Physics II, Faculty of Physics and Geosciences, University of Leipzig, Linnéstraße 5, 04103 Leipzig, Germany*
[2]*ON Semiconductor, Rožnov pod Radhoštem, Czech Republic*
(Received 26 November 2003; revised manuscript received 25 August 2004; published 19 January 2005)

We address and explain the occurrence of bulk and interface modes in zinc-blende group-III–group-V semiconductor layer structures observed by spectroscopic ellipsometry at infrared wavelengths. Fano- and Brewster-type transverse-magnetic (*p*-polarized) interface modes as well as transverse-electric (*s*-polarized) surface-guided interface modes are assigned by solutions of the surface polariton dispersion relations for polar semiconductor layer structures. We show that the Berreman-effect [D. W. Berreman, Phys. Rev. **130**, 2193 (1963)] is associated with the occurrence of a Fano-interface polariton. Experimental verification is demonstrated for a GaAs homostructure, which consists of differently Te-doped *n*-type substrates covered by undoped epilayers.

DOI: 10.1103/PhysRevB.71.035324 PACS number(s): 78.20.−e, 78.30.−j, 71.36.+c

I. INTRODUCTION

Semiconductor device structures consist of layers with different alloy compositions, individual dopant incorporation, free-charge-carrier properties, and eventually of complex structures with hundreds of interfaces. Novel metastable materials, unavailable from natural sources, can be grown atomic-layer-wise by modern nonequilibrium growth techniques. Determination of their physical properties is mandatory for the appropriate design of heterostructure devices. Demands for control and characterization of individual layer properties during and after deposition require adequate experimental techniques. Optical tools are noninvasive and nondestructive, and provide immediate access to fundamental physical parameters.

Ellipsometry is renowned for its precision and ability to measure the complex-valued optical dielectric function of thin films in complex layer structures.[1] In particular, the use of infrared (ir) ellipsometry proved very useful in exploration of lattice vibration modes, free-charge-carrier parameters, strain, composition, and chemical-ordering information from advanced semiconductors in complex layer structures, e.g., see Refs. 2–8. In many of the previous reports, polarized interface mode propagation effects remained unexplained. The aim of the present work is to demonstrate the physical origin of surface and interface modes in semiconductor layer structures, which can be observed by ir spectroscopic ellipsometry, and which provides very useful information on phonon and plasmon mode properties.

The link between the internal *linear* interactions (polaritons)[9] of light with matter and the externally observable changes of a probing electromagnetic radiation field (intensity, polarization state) is described by the frequency- and momentum-dependent complex-valued dielectric function ε. Heterointerfaces impose additional interface-bound polaritons, which descend from the bulk-supported polaritons of the adjacent media. Infrared polaritons involve lattice excitations with polar momentum and free-charge-carrier plasma modes. The ir optical response of layered structures composed of polar semiconductor materials is strongly influenced by resonant excitation of phonon- and plasmon-supported bulk and interface modes (*surface polaritons, surface guided waves*). Precise information on phonon and plasmon mode parameters can be obtained from measurement and model analysis of the frequency-dependent sample response, e.g., in terms of the complex reflectance ratio $\rho = r_p / r_s$, which consists of the reflection coefficients for light polarized parallel (r_p) and perpendicular to the plane of incidence (r_s). Ellipsometry can precisely determine $\rho = \tan \Psi \exp(i\Delta)$, $i = \sqrt{-1}$, where Ψ and Δ denote the ellipsometric parameters.

Most features within ir ellipsometry spectra are caused by bulk and interface modes, which depend on the behavior of ε of the involved materials. In particular, the resonance line shapes crucially depend on the absorption loss near the interface mode frequencies. Because ε depends on phonon and plasmon mode parameters, ir ellipsometry is extremely sensitive to lattice-vibration and free-charge-carrier properties of heterostructure constituents with film (layer) thickness less than a fraction of the probing wavelength.

In this paper, we discuss infrared bulk and interface modes in zinc-blende group-III–group-V semiconductor layer structures. We assign transverse-magnetic and transverse-electric modes by solutions of the surface polariton dispersion relations for polar semiconductor layer structures. Experiments on GaAs homostructures prove the occurrences of the interface modes, in excellent agreement with the outlined theory. The concept developed here will become useful for further ir ellipsometry studies on semiconductor heterostructures.

II. BULK AND INTERFACE POLARITONS IN SEMICONDUCTOR LAYER STRUCTURES

A. Bulk polaritons

Polaritons are the eigenstates of the system matter and radiation field, which obey Maxwell's postulates, and are seen as composite states of the photons and the elementary

matter excitations commonly designated as phonon polaritons, exciton polaritons, or magnon-polaritons, etc., depending on the predominant matter excitation.[10,11] For isotropic materials, the bulk polariton dispersion relation reads

$$\left(\frac{c\boldsymbol{k}}{\omega}\right)^2 = \varepsilon(\omega,\boldsymbol{k}). \tag{1}$$

For simplicity, it is assumed here that the dielectric function ε is independent of the wave vector $\boldsymbol{k}$, i.e., spatial dispersion effects are neglected, and that the magnetic permeability is unity.[12] In frequency regions where ε is independent of ω, the dispersion relation takes the well-known form

$$\omega = ck/\sqrt{\varepsilon}. \tag{2}$$

For the case of nondoped (intrinsic: *i*) GaAs with a single ir active phonon resonance, the ir dielectric function reads as follows:[13]

$$\varepsilon(\omega) = \varepsilon^{(\mathrm{L})}(\omega) = \varepsilon_\infty \frac{\omega_{\mathrm{LO}}^2 - \omega^2 - i\omega\gamma}{\omega_{\mathrm{TO}}^2 - \omega^2 - i\omega\gamma}, \tag{3}$$

where ω_{TO}, ω_{LO}, and γ denote the transverse- (TO) and longitudinal-optical (LO) mode frequency and lattice mode broadening parameter, respectively. The high-frequency dielectric constant is given by ε_∞. In the case of doped (e.g., *n*-type: *n*) GaAs, free-charge-carriers are present and contribute to the dielectric function by $\varepsilon^{(\mathrm{FC})}$,

$$\varepsilon(\omega) = \varepsilon^{(\mathrm{L})}(\omega) + \varepsilon^{(\mathrm{FC})}(\omega). \tag{4}$$

The classical Drude equation holds sufficiently for description of $\varepsilon^{(\mathrm{FC})}$. For single-species free-charge-carriers,[13,14]

$$\varepsilon^{(\mathrm{FC})}(\omega) = -\frac{\omega_p^2}{\omega(\omega + i\gamma_p)}. \tag{5}$$

The *unscreened* plasma frequency $\omega_p = e\sqrt{N/(\tilde{\varepsilon}_0 m)}$ depends on the free-charge-carrier concentration N, and their effective mass m ($\tilde{\varepsilon}_0$ is the vacuum permittivity and e is the electrical unity charge). The plasmon broadening parameter γ_p can be substituted by the carrier mobility $\mu = e/(m\gamma_p)$.[15]

For each k, two frequencies, $\omega_+(k)$ and $\omega_-(k)$, are solutions of Eq. (1) [bulk polaritons, dashed and dash-dotted lines in Fig. 1(b) for *n*- and *i*-type GaAs, respectively]. The two polariton branches ω_+ and ω_- for $k \to 0(\infty)$ approach 0 (ω_{TO}) and ω_{LO} (∞) for the case of *i*-type GaAs, or $\omega_{\mathrm{LPP}-}$ (ω_{TO}) and $\omega_{\mathrm{LPP}+}$ (∞) for the case of *n*-type GaAs. The roots of Eq. (4) are the frequencies of the coupled longitudinal optical-phonon plasmon modes ($LPP^{\pm}$),[16] which are bound by $0 < \omega_{\mathrm{LPP}-} < \omega_{\mathrm{TO}}$ and $\omega_{\mathrm{LO}} < \omega_{\mathrm{LPP}+} < \infty$, for $0 < \omega_p < \infty$ and $\gamma, \gamma_p \to 0$. In the frequency regions where $\varepsilon(\omega)$ is negative, no propagating normal mode exists. Total reflection will occur between $\omega = \omega_{\mathrm{TO}}$ and ω_+, and $\omega = 0$ cm^{-1} and ω_- for *n*-type GaAs, and between $\omega = \omega_{\mathrm{TO}}$ and ω_+ for *i*-type GaAs.

B. Surface polaritons and surface guided waves

The term surface[17] mode addresses phenomena which involve resonant propagation of electromagnetic (EM) waves and energy transport parallel to the surface. Surface guided waves (SGW) denote those waves with transverse-electric (TE; electric field vector parallel to interface) radiation fields. Such effects comprise total internal reflection and guided slab modes. Surface polaritons (SP) are interface-bound EM waves of transverse-magnetic (TM; magnetic field vector parallel to interface) character.

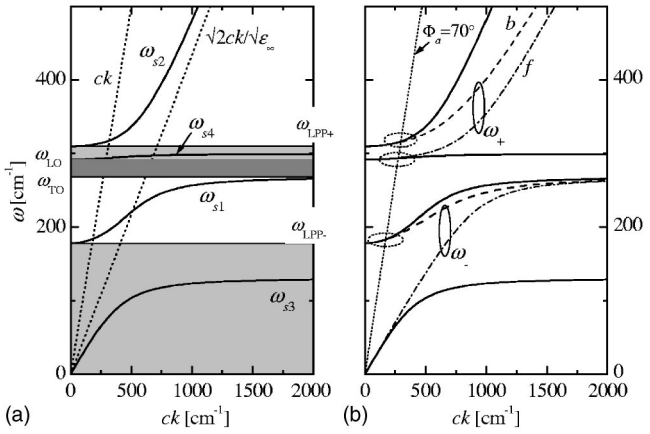

FIG. 1. (a) *SP* dispersions for the *i*-GaAs/*n*-GaAs interface (solid lines). The hatched areas indicate ω regions where either *n*-GaAs (gray; $0 \leqslant \omega \leqslant \omega_{LPP-}$ and $\omega_{\mathrm{TO}} \leqslant \omega \leqslant \omega_{LPP+}$), or *i*-GaAs (black: $\omega_{\mathrm{TO}} \leqslant \omega \leqslant \omega_{\mathrm{LO}}$) have negative dielectric function values. (b) Same as (a) with the bulk dispersion branches for both *n*-GaAs (dashed lines) and *i*-GaAs (dash-dotted lines) for comparison. (Parameters for GaAs are given in Table I.)

Surface polariton's at a single interface cannot be easily excited within a standard reflection or transmission experiment because their allowed dispersion range is to the right of the "light line" $\omega = ck$, and high-index-of-refraction prisms[18] are necessary to increase the wave vector of the incident light wave. However, dielectric properties of polar semiconductors at long wavelengths, bound within a thin-film structure, produce boundary conditions for certain wavelengths, where resonant excitation of SP's can be observed without use of a high-index prism. Berreman[19] was first to report the characteristic loss of the *p* reflectivity for a LiF film near the LiF LO mode frequency, when the film was backed by silver. It will be shown that this Berreman effect in polar semiconductor layer structures is caused by the excitation of a TM-polarized SP mode.[20,21] Furthermore the Brewster-type SP modes,[10,20] unnoticed so far in ir studies of semiconductor layer structures, will be discussed.

The occurrence of SP and SGW modes in polar semiconductor heterostructures is demonstrated here by calculations as well as by experiment. A brief derivation of the single- and double-interface polariton dispersion relations is given in the Appendix. Table I contains typical GaAs ir model parameters, which are used for the following calculations. The subsequent discussion holds for polar heterostructures as well (e.g., AlGaInP—GaAs), except for different material-related resonance frequencies. The plasma broadening values chosen here correspond to very high carrier mobility parameters [$\sim 5 \times 10^4$ cm^2/(Vs)], for better visibility of the SP and SGW effects within the calculated spectra. To begin with, the solution of Eq. (A2) is discussed for the *i*-GaAs(ε_f)/*n*-

TABLE I. GaAs lattice-mode and free-charge-carrier parameters used for the examples discussed in this section. The free-electron mass is m_0.

	ε_∞	ω_{TO} [cm^{-1}]	ω_{LO} [cm^{-1}]	γ [cm^{-1}]	$\log(N[\mathrm{cm}^{-3}])$ ω_p [cm^{-1}]	$\log(\mu[\mathrm{cm}^2(\mathrm{Vs})^{-1}])$	m [m_0]
ε_f	10.6	268	292	1.5	0		
ε_b	10.6	268	292	1	17.5	4.7	0.063[a]
					670	[b]	

[a]Reference 16.

[b]For the calculation of the SP and SGW dispersion in Fig. 2, no plasma broadening was assumed.

GaAs(ε_b) interface. The actual modes observable at the double-interface structure follow through numerical analysis of Eqs. (A8) and (A9). For simplicity, phonon and plasmon broadening is omitted for solving Eq. (A2). The dielectric functions are then

$$\varepsilon_b(\omega) = \varepsilon_\infty \frac{\omega_{\mathrm{LO}}^2 - \omega^2}{\omega_{\mathrm{TO}}^2 - \omega^2} - \frac{\omega_p^2}{\omega^2},$$

$$\varepsilon_f(\omega) = \varepsilon_\infty \frac{\omega_{\mathrm{LO}}^2 - \omega^2}{\omega_{\mathrm{TO}}^2 - \omega^2}, \tag{6}$$

where ε_∞, ω_{TO}, ω_{LO}, and ω_p denote the GaAs high-frequency dielectric constant, TO, LO, and plasmon-frequency parameters, respectively.

Equation (A2) has four physical roots,

$$\omega_{s1,2} = \frac{1}{2}\sqrt{s_+ \mp \sqrt{s_+^2 - 8\omega_{\mathrm{TO}}^2[s_+ - 2\omega_{\mathrm{LO}}]}}, \tag{7}$$

$$\omega_{s3,4} = \frac{1}{2}\sqrt{s_- \mp \sqrt{s_-^2 - 8\omega_{\mathrm{TO}}^2[s_- - 2\omega_{\mathrm{LO}}]}}, \tag{8}$$

with

$$s_\pm = \frac{2k_x^2}{\varepsilon_\infty} + 2\omega_{\mathrm{LO}}^2 + \frac{\omega_p^2}{\varepsilon_\infty} \pm \sqrt{\frac{4k_x^4 + \omega_p^4}{\varepsilon_\infty^2}}. \tag{9}$$

It is worthwhile to consider the small and large wave-vector behavior of the four solutions. Branches ω_{s1}, ω_{s2}, and ω_{s4} approach ω_{LPP-}, ω_{LPP+}, and ω_{LO} when $k \to 0$, respectively, whereas $\omega_{s3} \sim ck/\sqrt{\varepsilon_\infty}$. Note that ω_{s3} would also remain finite at $k=0$ when ε_f contains a plasma term different from that in ε_b. For $k \to \infty$, $\omega_{s1} \to \omega_{\mathrm{TO}}$, and $\omega_{s2} \sim ck/\sqrt{2/\varepsilon_\infty}$, whereas

$$\omega_{s3,4}^{k\to\infty} = \frac{1}{2}\sqrt{2\omega_{\mathrm{LO}}^2 + \frac{\omega_p^2}{\varepsilon_\infty} \mp \sqrt{\left(2\omega_{\mathrm{LO}}^2 + \frac{\omega_p^2}{\varepsilon_\infty}\right)^2 - 8\omega_{\mathrm{TO}}^2\frac{\omega_p^2}{\varepsilon_\infty}}}. \tag{10}$$

Accordingly, modes ω_{s1}, ω_{s2} obey strong dispersion, whereas ω_{s4} is bound within a very small frequency region. Figure 1(a) depicts the SP dispersions and their boundaries.

The particular type of the SP mode is determined by the nature of the dielectric functions of the two media. The hatched areas in Fig. 1(a) indicate the frequency regions in which either ε_b or ε_f are negative. From there it is obvious that ω_{s1}, ω_{s2} and ω_{s3}, ω_{s4} belong to situations (SP2) and (SP1) discussed in the Appendix, and are referred to as Brewster (BSP) and Fano (FSP) modes, respectively. The mode associated with ω_{s4} causes the Berreman effect. Figure 1(b) shows the bulk dispersion branches for both *n*-GaAs (dashed lines) and *i*-GaAs (dash-dotted lines) for comparison. Branches ω_{s1} and ω_{s2} (ω_{s3} and ω_{s4}) follow closely those of the bulk dispersion ω_- and ω_+, label *b* and the dashed lines, for the *n*-GaAs (label *f*, dash-dotted lines, for the *i*-GaAs) for small *k*, and remain always above (below) the bulk polariton dispersion, respectively. Due to the presence of the free-charge-carriers, both bulk polariton *n*-GaAs branches are now active for the "light line." The SP branches ω_{s1} and ω_{s2} remain above the bulk polariton branches of the *n*-GaAs, whereas ω_{s3} and ω_{s4} are found below the *i*-GaAs bulk polariton branches [Fig. 1(b)]. Accordingly, the wave-vector *x* components are smaller (larger) than the associated bulk modes at the same frequency.

No intersection exists between SP and bulk polariton branches [Fig. 1(b)]. The SP modes are nonradiant. However, if one medium is terminated by a second interface (thin film), and bound by a third medium (ε_a) through which the interface between ε_b and ε_f can be illuminated, the SP branches are modified by a small wave-vector shift Δk_x. As a result,

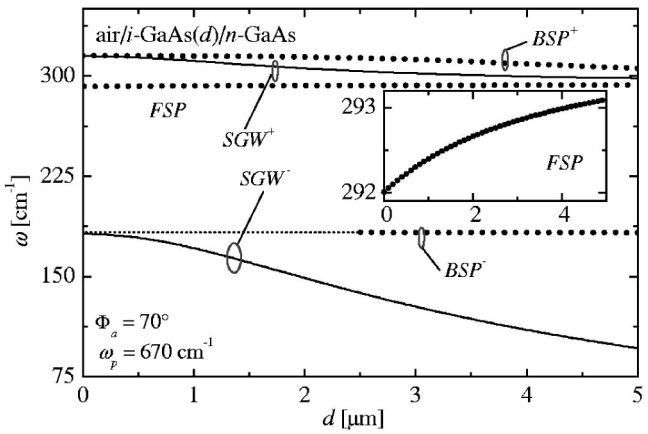

FIG. 2. SP (TM-polarized, dotted lines: FSP, BSP$^{+,-}$) and SGW (TE-polarized, solid lines: SGW$^{+,-}$) mode frequencies for the air/*i*-GaAs(d)/*n*-GaAs thin-film structure as a function of the film thickness d. The frequencies for the SP and SGW modes follow from numerical evaluation of Eqs. (A8) and (A9), respectively. The inset enlarges the FSP mode dependence versus thickness. Parameters used are given in Table I.

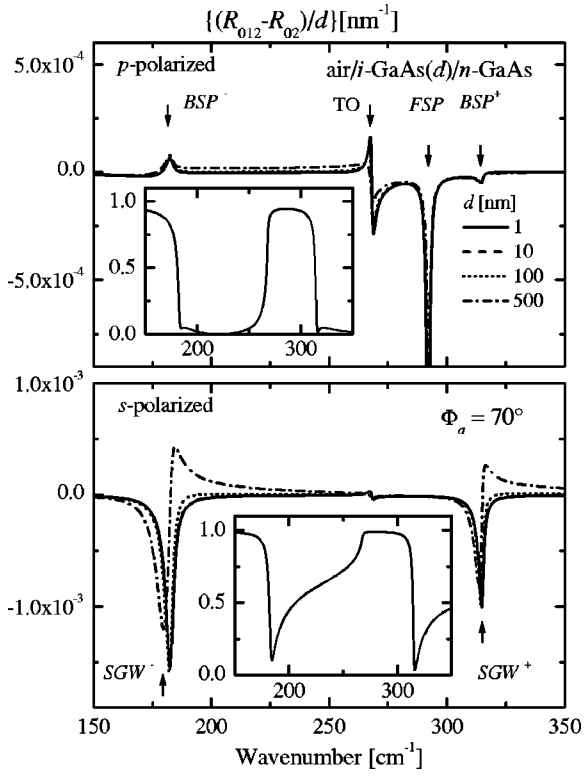

FIG. 3. Calculated reflection coefficient (R_{012} for the three-phase system in Fig. 8) differences for *p*- (upper panel) and *s*-polarized plane waves (lower panel) for an air/*i*-GaAs(*d*)/*n*-GaAs structure with different thickness *d* (phase 0: air, phase 1: *i*-GaAs film, phase 2: *n*-GaAs substrate). The differences are divided by *d* in units of nm. (The parameters for calculation of ε_f and ε_b are given in Table I.)

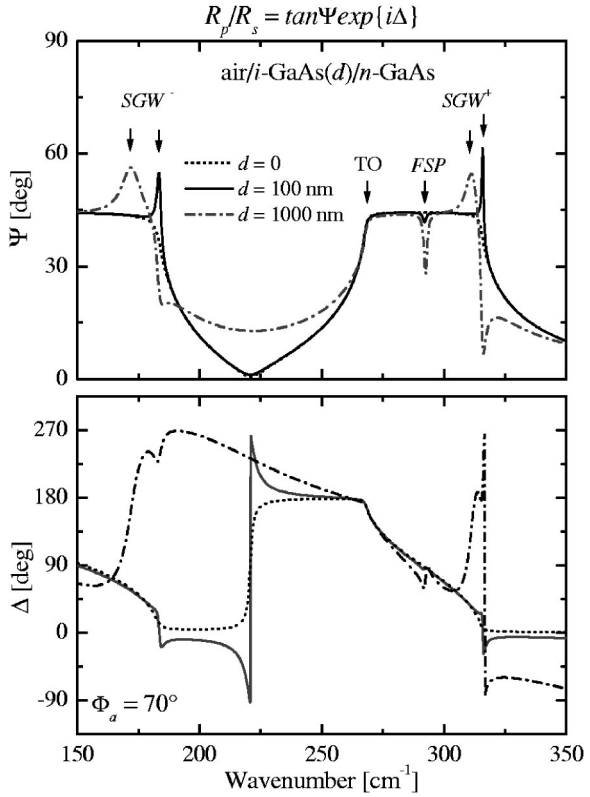

FIG. 4. Same as Fig. 3 for Ψ (upper panel) and Δ (lower panel), and for $d=0$, 100 nm, and 1000 nm. The SGW mode shift with *d* is obvious, as is also the occurrence of the FSP mode. Resonance due to modes BSP are hard to detect because their effects are subsumed by the strong changes in the *s* polarization due to the SGW modes and due to the bulk polariton mode excitation.

the branches ω_{s1}, ω_{s2}, and ω_{s4} become active and can be observed upon illuminating the structure with light, as will be demonstrated below.[22]

Figure 2 depicts numerical solutions of the minima in in Eqs. (A8) and (A9) versus the film thickness *d*. Three SP branches emerge at frequencies ω_{s1}, ω_{s2}, and ω_{s4} shown in Fig. 1(a). According to the above definition, those bound by ω_{s1}, ω_{s2} for $d\rightarrow 0$ are termed here BSP^- and BSP^+, and the mode bound by ω_{s4} is termed FSP. Note that ω_{s1}, ω_{s2} are bound by the lower and upper LPP modes within the *n*-GaAs, from where the " $^-$" and " $^+$"in $BSP^{+,-}$ is adopted. The mode FSP is the cause of the Berreman effect. The minimum in Eq. (A8) for mode BSP^- is weak for small thickness *d*, and drawn here as a thin dotted line. All SP modes undergo slight changes with increasing *d*, and the inset enlarges that for FSP. Two SGW modes occur with strong thickness dependence. Both SGW branches merge with modes $BSP^{+,-}$ for $d\rightarrow 0$, and are therefore termed $SGW^{+,-}$ accordingly. Because ω_{s1} and ω_{s2} depend on ω_p, modes $BSP^{+,-}$ and $SGW^{+,-}$ are extremely sensitive to the free-charge-carrier concentration.

Figure 3 depicts calculated *p*- and *s*-polarized reflection coefficients $R_{p,s}=|r_{p,s}|^2$ for the thin-film example, and Fig. 4 presents those for the ellipsometric parameters Ψ and Δ as a function of ω in units of cm^{-1}, for various film thicknesses *d*, and at $\Phi_a=70°$. The reflection coefficients for the bare substrate are shown in the insets, and for the ellipsometric parameters as dotted lines in Fig. 4. The parameters γ and μ used for calculations shown in Figs. 3 and 4 are now as shown in Table I. The modes in Fig. 2 can now be identified within the data and are indicated by vertical arrows (FSP, $BSP^{+,-}$, $SGW^{+,-}$) in Figs. 3 and 4.

(i) FSP. The changes in $R_{p,s}$, Ψ, and Δ imposed by the thin *i*-GaAs layer are extremely small, except for the strong resonance, denoted by FSP, which occurs near ω_{LO}. This situation, obtained here for a polar semiconductor film structure near $\omega \geqslant \omega_{\mathrm{LO}}$, is identical with that under which Berreman reported the loss of the *p* reflectivity of a LiF film near the LiF LO mode frequency when the film was backed by silver.[19] This effect has been termed the "Berreman effect," which is frequently interpreted as due to a resonant excitation of LO lattice modes within the film (see, e.g., Chap. 10 in Kittel, *Solid State Physics*, Ref. 13). It is, however, evident from the above discussion that the SP situation is not related to a LO lattice mode vibration, because the associated EM displacement pattern across the film is that of a TM mode with propagation direction parallel to the film interfaces. This SP mode is a lossy Fano mode, because both ε_b and ε_a are complex-valued due to γ and μ. It can be shown that the width of the line shape is directly related to $\mathrm{Im}\{\varepsilon_f\}$, and

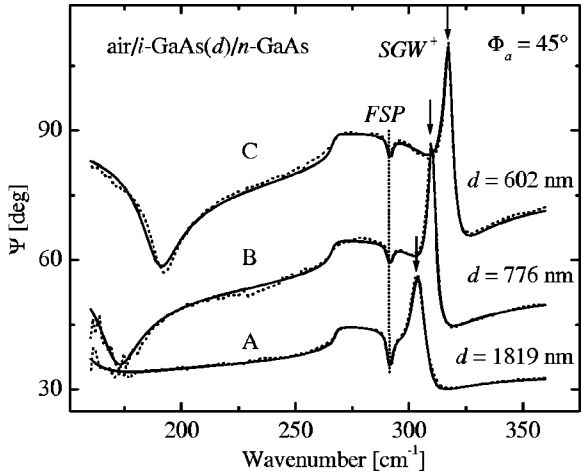

FIG. 5. Observation of Fano (FSP; vertical dotted line) and SGW^+ modes (vertical arrows) in semiconductor homostructures: Experimental (dashed lines) and best-fit (solid lines) Ψ spectra from three different *i*-GaAs/*n*-GaAs(Te-doped) samples with thickness *d*, and slightly varying free-charge-carrier concentration *N*, and mobility μ (Table II). Spectra for samples *B* and *C* are shifted by 20° and 40° for convenience, respectively.

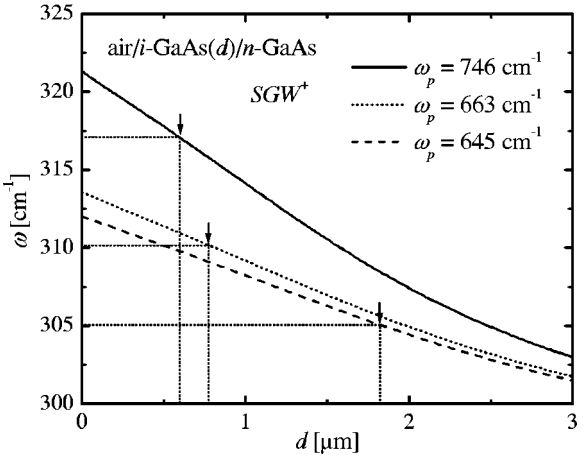

FIG. 6. Calculated thickness dependence of the SGW^+ mode for the plasma frequency values in the *i*-GaAs(*d*)/*n*-GaAs samples studied in Fig. 5. The arrows indicate the observed frequencies, which provide exactly the thickness values obtained for the *i*-GaAs film in samples *A*, *B*, and *C* from the best-fit shown in Fig. 5.

presents an extremely sensitive measure for small absorption within the film.[23,24] If both components of the GaAs—GaAs film structure would be doped, but with different free-charge-carrier concentrations, for the situation discussed here, the mode FSP would split into modes $FSP^{-,+}$ occurring near the film modes ω_{LPP-}, ω_{LPP+}, respectively.

(ii) BSP. The *p* reflectivity is further affected by subtle changes, upon increase in *d*, at frequencies near $\omega_{s1}(k=0) = \omega_{LPP-}$ (BSP^-) and $\omega_{s2}(k=0) = \omega_{LPP+}$ (BSP^+). The subtle modes with Lorentzian line shape in R_p refer to situation (*SP*2). It is likely that such small resonance effects will fall within the experimental error bars. Their experimental observation was not yet reported.

(iii) SGW. Strong changes occur within the *s*-polarized reflectivity upon an increase in *d*. The frequency shift of the modes termed $SGW^{-,+}$ agrees excellently with their dispersion shown in Fig. 2. The upward-pointed peaks in Ψ reveal this shift most clearly. Note that the frequencies of these modes separate from the bulk polariton mode frequencies as *d* increases. The bulk polariton excitation causes the sudden drop in *p* and *s* reflectivity above the frequencies where the "light line" in Fig. 1(b) crosses the branches $\omega_{-,+}$.

III. EXPERIMENT

The measurements shown in the following section were obtained using "in-house built" Fourier-transform-based ellipsometer systems for ir ($\lambda \sim 100-15$ μm) wavelengths. Ellipsometry data analysis was discussed in detail previously, and the interested reader may refer to Refs. 1 and 24–29. Samples with a single *i*-GaAs film deposited by metal-organic vapor phase epitaxy using standard precursors and growth conditions on *n*-GaAs substrates are studied.

IV. RESULTS

Figure 5 presents experimental Ψ spectra for three *i*-GaAs(*d*)/*n*-GaAs(ω_p, γ_p) film structures, with different film thickness *d*, plasma frequencies ω_p, and plasma broadening parameters γ_p caused by slightly different free-charge-carrier concentration and mobility parameters within the Te-doped *n*-GaAs substrates (see Table II). Resonant excitations of the FSP and the SGW^+ modes occur, according to the explanation given above. The FSP mode, which occurs slightly above the film LO frequency, is virtually unaffected by the thickness and the carrier concentration, as expected. The SGW^+ modes are shifted to higher wave numbers with increasing plasma frequency (increasing carrier concentration) because ω_{s2} shifts to higher frequencies, but also shifted to lower wave numbers with increasing thickness *d*, as shown in Fig. 6. The actual frequency shift is the sum of both effects, depending on *d* and ω_p. The modes SGW^- are overdamped and do not occur, because of the lattice and plasma broadening, which leads to stronger absorption in ε_b near the frequencies ω_{LPP-} compared to that near ω_{LPP+}.

Figure 6 depicts the SGW^+ mode frequency as a function of *d* for the plasma frequency values obtained from the best-fit analysis of the experimental data in Fig. 5. The branches are shifted to higher frequencies with increasing ω_p. The arrows indicate the peak positions of the features labeled by SGW^+ in Fig. 5. The intersections with the according function $SGW^+(d, \omega_p)$ provide the thickness of the *i*-GaAs layer

TABLE II. Sample parameters obtained for the examples shown in Fig. 5.

Sample	d	$N \times 10_{17}$ [cm^{-3}]	μ [cm^2/(Vs)]
A	2145	3.39	2750
B	761	3.5	2450
C	602	4.47	2290

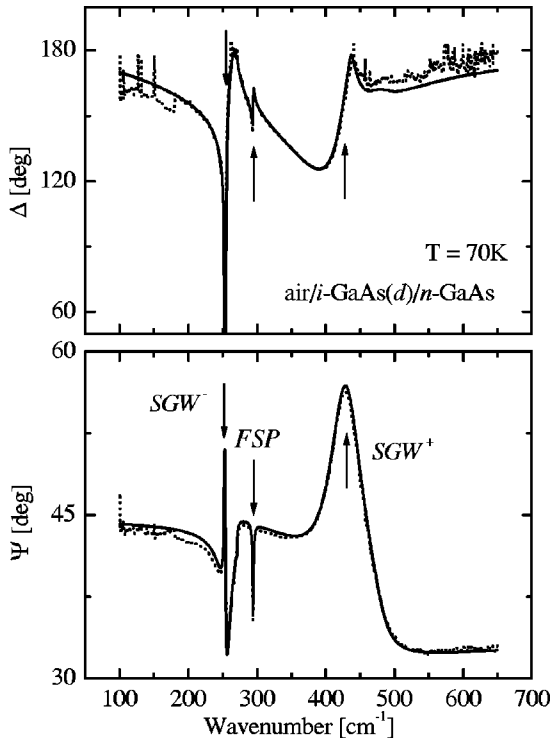

FIG. 7. Low-temperature (T=70 K) experimental (dashed lines) and best-fit (solid lines) calculated Ψ and Δ spectra from an undoped GaAs layer (675 nm) deposited on Te-doped *n*-type GaAs ($\Phi_a=70°$).

for all three samples, in excellent agreement with the best-fit thickness obtained from the line-shape fit of the ellipsometry data.

Figure 7 depicts ellipsometry data from a sample with $\omega_p=(1485\pm0.5)$ cm^{-1} [$N=(1.774\pm0.002)\times10^{18}$ cm^{-3}] at $T=70$ K. At low temperatures the lattice broadening parameter decreases from 1.5 cm^{-1} (300 K) to 0.6 cm^{-1} (70 K). For this sample we obtain $\mu=(2630\pm5)$ cm^2/(Vs) [$\gamma_p=(49.5\pm0.2)$ cm^{-1}] and $d=(657\pm1)$ nm. Due to the higher free-electron concentration in the substrate and the smaller lattice broadening parameter compared with the samples in Fig. 5, both the SGW$^-$ and the SGW$^+$ modes are blueshifted because of the increase in N, and are resonantly excited, as can be clearly seen here. The FSP mode is not affected by the substrate carrier concentration, which is about one order of magnitude larger here than in Fig. 5. This reflects the fact that the FSP mode descends from ω_{s4}, which is bound by the film LO frequency ω_{LO} for $k\rightarrow0$ [Eq. (8)].[30]

V. DISCUSSION

The Berreman effect was often addressed in discussions of *p*-polarized reflection or transmission studies of polar or conductive material layer structures.[31–35] Berreman[19] explained his original observation by the resonant absorption of ir radiation within the film *at* wavelengths equivalent to the LiF-LO phonon mode frequency. The interpretation of this observation reads in contemporary textbooks as if light is absorbed *by* resonant excitation of the thin-film LO modes.[13] After the Fourier-transform-based ir ellipsometry technique became available, owing to the pioneering work of Röseler,[27] the Berreman effect gained new attention. Observations of this effect are often reported for polar material layer structures when an ir active longitudinal phonon mode is within the wave-number region under study.[4,6,7,36–40]

Harbecke *et al.*[33] stated on the basis of intuitive arguments that the Berreman effect is caused by surface charges due to the normal component of the electric field, where the maximum in the dielectric loss function near the LO frequency determines the frequency of the Berreman resonance. The energy transport phenomenon related to the interface polariton excitation was not recognized. Röseler[27] pointed out that fundamental problems exist with the interpretation currently given in Kittel.[13] Following the derivation given by Harbecke *et al.*,[33] Röseler analyzed the surface polariton dispersion relation for the double-interface situation when the film is a polar medium (the dielectric function is described by a harmonic oscillator) and the half-infinite medium is a metal demonstrating that the Berreman feature is not due to resonant LO mode excitation (implementing that there is no electromagnetic field absorption in the film), but caused by an interference optical effect with energy transported along the interface. The fact that both layer and substrate must reveal small absorption coefficients for the effect to become observable was also pointed out. Multiple local minimums versus d exist in Eq. (A8) for the polar film on metal. The first one coincides with the so-called Berreman thickness,[33] the value d for which the resonance dip in R_p is strongest. For much smaller thickness, the frequency of the minimum in Eq. (A8) is shifted to shorter wave numbers. The frequency of the latter mode was interpreted as that of a true SP mode, which was thought to be different from the Berreman mode. However, as shown in Fig. 2, for semiconductor layer structures the FSP mode frequency [solutions of type (SP1)] for Eq. (A8) is a continuous function of d. The two different modes identified by Röseler can be well understood as being due to the same SP mode branch.

Humlíček, as well as Zollner *et al.*, adopted, in principle, Röseler's assignment of the Berreman effect as that of a pure interference-optical phenomenon, backed by interpretations of ir ellipsometry experiments done on LiF films deposited on silver and on silicon,[37] as well as by experiments done on nondoped 4H-SiC films deposited on heavily doped 4H-SiC substrates.[38] Humlíček favored Röseler's view extending it by the "intensified-absorption-loss" as the cause of the Berreman effect.[37,41] Humlíček calculated the intensity of the electric field E inside the LiF film near the substrate and near the ambient interface, and compared those to calculated reflectivity differences with and without the film. He found that a quantity proportional to $\mathrm{Im}\{\varepsilon_f\}d/\lambda|E|^2$ was in very good agreement with the reflectivity intensity differences, and where λ is the ir wavelength. Because $\mathrm{Im}\{\varepsilon_f\}|E|^2$ is proportional to the absorption loss within a material, the conclusion was made that the Berreman resonance near the LO frequency is caused by an "electric field enhanced" intensified absorption loss. The intensified electric field was explained as an interference optical phenomenon at a wavelength where the index of refraction is less than 1, and where the field inside the film is composed of back and forward trav-

eling waves. Zollner *et al.*[38] reported the observation of the Berreman effect within ir ellipsometry studies of nondoped epitaxial 4H-SiC on heavily doped 4H-SiC homostructures. Attempts to explain this effect were made. However, the physical origin of the Berreman effect in their data remained somewhat unclear.[42]

Two critical issues remained, namely that interference should be ineffective across interfaces separated by a very small fraction of the probing wavelength λ only, and that absorption must exist for the effect to be observable. For example, the FSP mode in Fig. 3 occurs regardless of the actual thickness d, as long as d is small. An appreciable change in R_p (or Ψ and Δ) could already be measured for $d \approx 1$ nm. For GaAs, this mode occurs for $\lambda \sim 35$ μm. It was now discussed in this paper that the cause of the observed resonance loss is due to the excitation of a Fano-type surface polariton mode. This mode is accompanied by energy transport along the interface, and accommodates absorption loss within the layer structures by homogeneous and inhomogeneous broadening of the polar lattice modes, as well as by scattering. Accordingly, a loss of the reflected (or transmitted) p-polarized light intensity at oblique incidence is detected.

We note finally that the p- and s-polarized interface mode phenomena addressed in this work play a crucial role in detection of magneto-optic free-charge-carrier-induced birefringence at ir or far-ir wavelengths.[43] There, coupling of bulk and interface polaritons with circularly polarized free-charge-carrier helicons causes subtle anisotropy upon splitting of the interface mode branches. Detailed discussion of the magneto-optic interface polaritons will be given somewhere else.

VI. SUMMARY

The ir response of polar semiconductor layer structures is strongly influenced by excitation of bulk and interface polariton modes. We have identified Fano-, Brewster-, and surface-guided interface modes upon solution of the surface polariton dispersion relation for layered structures. Fano- and surface-guided modes are observed by experiment. These modes are tied to the properties of lattice phonon and plasmon modes. The explanation for the physical origin of the Berreman effect was given. Spectroscopic ellipsometry is an excellent technique for studying polariton properties in zinc-blende group-III–group-V semiconductor layer structures. Upon model calculations, contributions to the dielectric function due to ir-active polar phonon modes and coupled longitudinal-phonon-plasmon modes can be differentiated and quantified for individual constituents in layered heterostructures.

ACKNOWLEDGMENTS

This work was supported in part by DFG Grants No. Rh 28/3-1,2, No. SCHUH 1338/3-1, and No. SCHUH 1338/4-1, in part by NSF Contract No. DMI-9901510, and in part by the Federal Ministry of Education and Research of the Federal Republic of Germany within the Funding scheme "Innovative regionale Wachstumskerne." M.S. and T.H. thank Daniel W. Thompson and Professor Dr. John A. Woollam, UNL for further support. We also wish to thank Dr. Craig M. Herzinger and Dr. Thomas E. Tiwald, J.A. Woollam Co., Inc., 645 M Street, Suite 102, Lincoln, NE 68508, for their help and stimulating discussions.

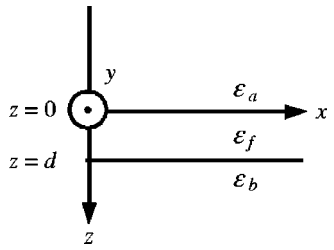

FIG. 8. Two half-infinite media (three-phase system) with dielectric functions ε_a (ambient) and ε_b (substrate), embrace a dielectric film of thickness d with dielectric function ε_f.

APPENDIX: INTERFACE DISPERSION RELATION

The denominators of the Fresnel reflection coefficient for p- and s-polarized light, r_p and r_s, respectively, provide a convenient form of the dispersion for the interface-bound TM or TE modes in thin-film heterostructures,[23] and shall be studied here. The coordinate system is shown in Fig. 8.

1. SP's at the single interface (bound TM waves)

For the single interface, the p-polarized Fresnel reflection coefficient can be rearranged into

$$0 = \frac{k_{z,1}}{\varepsilon_1} + \frac{k_{z,2}}{\varepsilon_2}, \tag{A1}$$

where $\varepsilon_1, k_{z,1}$ and $\varepsilon_2, k_{z,2}$ are the complex dielectric functions of the materials and wave vector z components on both sides of the interface. The associated x component of the wave vector can be expressed as

$$k_x^0 = \frac{\omega}{c}\left(\frac{\varepsilon_1 \varepsilon_2}{\varepsilon_1 + \varepsilon_2}\right)^{1/2}. \tag{A2}$$

The associated z components within the ith media are

$$k_{z,i} = \left[\left(\frac{\omega}{c}\right)^2 \varepsilon_i - (k_x^0)^2\right]^{1/2}. \tag{A3}$$

For a *bound* TM wave, the associated electric fields must be evanescent on both sides of the interface, and the $k_{z,i}$'s must possess imaginary parts. In case of no or only little absorption, i.e., $\mathrm{Im}(\varepsilon_1) \sim \mathrm{Im}(\varepsilon_2) \sim 0$, Eq. (A1) is fulfilled in two different situations:

(SP1): $k_{z,1}$ and $k_{z,2}$ are imaginary, and $\mathrm{sgn}(\varepsilon_1) = -\mathrm{sgn}(\varepsilon_2)$ (Fano modes).

(SP2): $k_{z,1}$ and $k_{z,2}$ are real, $\mathrm{sgn}(k_{z,1}) = -\mathrm{sgn}(k_{z,2})$, and $\varepsilon_1 > 0$ and $\varepsilon_2 > 0$ (Brewster modes).

The modes in situation (SP1) are called Fano modes and correspond to surface TM waves, which propagate along the interface and decay exponentially to zero as $z \to \pm\infty$. The SP

modes in situation (SP2) have been termed Brewster modes for which the intensity of the reflected wave is zero or minimal (see, e.g., Ref. 10) and which, in contrast to the Fano modes, do not attenuate with distance from the interface. The Fano modes cannot linearly couple to the bulk modes, and are nonradiant.[10,11]

2. Double interface SP's (bound TM waves)

The existence of a second interface (Fig. 8), separated from the first interface by a fraction of the probing wavelength only ($d \ll c/\omega$), causes a subtle shift Δk_x of the x component of the wave vector k_x^0, where k_x^0 may refer to a solution of Eq. (A2) for either interface.[23] The new SP resonance occurs at $k_x^0 + \Delta k_x$, where the shift Δk_x can be expressed through the substrate (ε_b) and film (ε_f) dielectric functions, the film thickness d, k_x^0, and the p reflectivity of the ambient-film interface r_{p01}^0 at k_x^0 (Refs. 23 and 24),

$$\Delta k_x = 2 r_{p01}^0 k_x^0 \frac{\varepsilon_f \varepsilon_b}{(\varepsilon_f + \varepsilon_b)(\varepsilon_f - \varepsilon_b)} e^{i2\alpha_0}, \tag{A4}$$

with

$$\alpha_0 = \frac{\omega}{c} d \sqrt{\frac{\varepsilon_f}{\varepsilon_f + \varepsilon_b}}, \tag{A5}$$

$$r_{p01}^0 = \frac{\sqrt{\varepsilon_f}\cos\Phi_a - \sqrt{\varepsilon_a}\cos\Phi_f}{\sqrt{\varepsilon_f}\cos\Phi_a + \sqrt{\varepsilon_a}\cos\Phi_f}, \tag{A6}$$

and $\cos\Phi_{a,f}$ obtained from Snell's law,

$$\cos\Phi_i = \sqrt{1 - \frac{\varepsilon_a \varepsilon_f}{\varepsilon_i(\varepsilon_a + \varepsilon_f)}}, \quad i = \text{“}a,\text{”“}f\text{.”} \tag{A7}$$

Due to this shift, the individual interface SP wave-vector dispersions are displaced, and may cross the individual bulk polariton branches, and the new SP wave-vector x component is complex-valued. Hence, the associated z components are complex as well, and light mediated through one of the media into the interface can excite the SP mode, which will decay exponentially away from the interface. Unfortunately, the ω dependence of $k_x^0 + \Delta k_x$ cannot be solved explicitly, and has to be evaluated numerically. It is, however, more efficient and accurate to use the denominator of the p-polarized reflection coefficient for this purpose,

$$F_{\mathrm{TM}} = 1 + r_{p01} r_{p12} e^{i2\alpha_0}, \tag{A8}$$

which is identical to the TM mode condition, and which should vanish near an SP resonance.

3. Double interface SGW's (bound TE waves)

Similar to the case above, the relation for TE interface waves (SGW) at a thin film follows from the denominator of the s-polarized reflection coefficient (Ref. 24),

$$F_{\mathrm{TE}} = 1 + r_{s01} r_{s12} e^{i2\alpha_0}, \tag{A9}$$

which must also vanish near an SGW resonance.

*Electronic address: mschub@physik.uni-leipzig.de; URL: http://www.uni-leipzig.de/ellipsometrie

[1] D. E. Aspnes, in *Handbook of Optical Constants of Solids*, edited by E. D. Palik (Academic, New York, 1998).

[2] T. E. Tiwald, J. A. Woollam, S. Zollner, J. Christiansen, R. B. Gregory, T. Wetteroth, S. R. Wilson, and A. R. Powell, Phys. Rev. B **60**, 11 464 (1999).

[3] T. Hofmann, V. Gottschalch, and M. Schubert, Phys. Rev. B **66**, 195204 (2002).

[4] J. Humlíček, R. Henn, and M. Cardona, Appl. Phys. Lett. **69**, 2581 (1996).

[5] C. Bundesmann, M. Schubert, D. Spemann, T. Butz, M. Lorenz, E. M. Kaidashev, M. Grundmann, N. Ashkenov, H. Neumann, and G. Wagner, Appl. Phys. Lett. **81**, 2376 (2002).

[6] M. Schubert, B. Rheinländer, E. Franke, H. Neumann, T. E. Tiwald, J. A. Woollam, J. Hahn, and F. Richter, Phys. Rev. B **56**, 13 306 (1997).

[7] A. Kasic, M. Schubert, S. Einfeldt, D. Hommel, and T. E. Tiwald, Phys. Rev. B **62**, 7365 (2000).

[8] A. Kasic, M. Schubert, Y. Saito, Y. Nanishi, and G. Wagner, Phys. Rev. B **65**, 115206 (2002).

[9] The term "polariton," originally introduced by Hopfield[44] to describe the "uncoupled polarization field particles" of a medium, was later designated to the coupled polarization excitation-photon modes[10] and further generalized by Mills and Burstein to include the coupled magnetic dipole excitation modes in magnetic media as well.[11]

[10] *Polaritons*, edited by E. Burnstein and F. de Martini (Pergamon Press, New York, 1974).

[11] D. L. Mills and E. Burstein, Rep. Prog. Phys. **37**, 817 (1974).

[12] For instance, in a free-electron plasma, the free-charge-carrier contribution to the dielectric function is no longer determined by the local electric field but is influenced by the field along the path, which the electrons travel when their mean free path or cyclotron radius exceeds the wavelength of the excitation. Such nonlocal effects can be observed in thin foils of alkali metals, and require a nonlocal $\boldsymbol{k}$-dependent form of the dielectric function as suggested by Lindhard.[45] In general, the wave-vector dependence of the dielectric function arises from the wave-vector dependence of the physical quantities that affect the dielectric function, such as ε_∞, ω_{TO}, ω_{LO}, and so on. A discussion of spatial dispersion effects on bulk and interface polaritons is given by D.L. Mills in Ref. 10, p. 147. One may also refer to the interesting paper by A. R. Melnyk in Ref. 10, p. 221, and references therein.

[13] C. Kittel, *Introduction to Solid States Physics* (Wiley, New York, 1986).

[14] C. Pidgeon, in *Handbook on Semiconductors*, edited by M. Balkanski (North-Holland, Amsterdam, 1980).

[15] C. M. Wolfe, N. Holonyak, and G. E. Stillmann, *Physical Prop-*

erties of Semicoductors (Prentice Hall, Englewood Cliffs, NJ, 1989).

[16] P. Yu and M. Cardona, *Fundamentals of Semiconductors* (Springer, New York, 1999).

[17] The surface of a sample may also be treated as an interface, and the terms "*surface*" and "*interface*" have the same meaning here.

[18] Such arrangements include the well-known "Otto" and "Kretschmann" configurations.[46–48]

[19] D. W. Berreman, Phys. Rev. **130**, 2193 (1963).

[20] U. Fano, J. Opt. Soc. Am. **31**, 213 (1941).

[21] H. Wolter, *Handbuch der Physik, Bd XXIV* (Springer, Berlin, 1965).

[22] The alternative for observation of SP modes is the use of a high-index prism, where the evanescent field at the base of the prism is brought close to the interface of interest. Thereby, the wave vector of the field coupled into the system is larger than the allowed bulk modes, and resonant excitation of SP modes can be observed upon loss of the *p*-polarized light intensity transmitted through the symmetric prism.[46,47]

[23] H. Raether, *Surface Plasmons* (Springer, Berlin, 1988).

[24] M. Schubert, *Infrared Ellipsometry on Semiconductor Layer Structures: Phonons, Plasmons and Polaritons* (Springer, Berlin, 2004).

[25] R. M. Azzam and N. M. Bashara, *Ellipsometry and Polarized Light* (North-Holland Publ. Co., Amsterdam, 1984).

[26] M. Schubert, T. E. Tiwald, and C. M. Herzinger, Phys. Rev. B **61**, 8187 (2000).

[27] A. Röseler, *Infrared Spectroscopic Ellipsometry* (Akademie-Verlag, Berlin, 1990).

[28] G. E. Jellison, Thin Solid Films **313–314**, 33 (1998).

[29] M. Schubert, in *Introduction to Complex Mediums for Optics and Electromagnetics*, edited by W. S. Weiglhofer and A. Lakhtakia (SPIE, Bellingham, 2003).

[30] The phonon mode frequencies change with temperature due to the thermal lattice expansion, which were obtained for this sample as $\omega_{TO}=(270.4\pm0.1)$ cm^{-1}, $\omega_{LO}=(292.3\pm0.2)$ cm^{-1}.[49]

[31] G. Mirjalili, T. J. Parker, S. F. Shayesteh, M. M. Bulbul, S. R. P. Smith, T. S. Cheng, and C. T. Foxon, Phys. Rev. B **57**, 4656 (1998).

[32] M. D. Sciacca, A. J. Mayur, E. Oh, A. K. Ramdas, S. Rodriguez, J. K. Furdyna, M. R. Melloch, C. P. Beetz, and W. S. Yoo, Phys. Rev. B **51**, 7744 (1995).

[33] H. Harbecke, B. Heinz, and P. Grosse, Appl. Phys. A: Solids Surf. **38**, 263 (1985).

[34] A. J. McAlister and E. A. Stern, Phys. Rev. **132**, 1599 (1963).

[35] H. Mayer and L. D. Blanaru, Z. Phys. **249**, 424 (1972).

[36] E. Wold, J. Bremer, O. Hunderi, J. M. Frigerio, G. Parjadis, and J. Rivory, J. Appl. Phys. **75**, 1739 (1994).

[37] J. Humlíček, Phys. Status Solidi B **215**, 155 (1999).

[38] S. Zollner, J. P. Carrejo, T. E. Tiwald, and J. A. Woollam, Phys. Status Solidi B **208**, R3 (1998).

[39] J. Šik, M. Schubert, T. Hofmann, and V. Gottschalch, MRS Internet J. Nitride Semicond. Res. **5**, 3 (2000).

[40] G. Leibiger, V. Gottschalch, and M. Schubert, J. Appl. Phys. **90**, 5951 (2001).

[41] J. Humlíček, Thin Solid Films **313–314**, 687 (1998).

[42] Interestingly, the data shown from the 4H—SiC homostructure in Fig. 1 of Ref. 38 clearly revealed a resonance structure at wave numbers above the Berreman effect, which resembles that of the SGW^+ mode discussed here for the GaAs homostructure. This resonance was not further commented on by the authors, but can now, in view of the above discussion, be identified with the occurrence of the SGW^+ mode resonance.

[43] M. Schubert, T. Hofmann, and C. M. Herzinger, J. Opt. Soc. Am. A **20**, 347 (2003).

[44] J. J. Hopfield, Phys. Rev. **112**, 1555 (1958).

[45] J. Lindhard, K. Dan. Vidensk. Selsk. Mat. Fys. Medd. **8**, 28 (1954).

[46] A. Otto, Z. Phys. **216**, 398 (1968).

[47] E. Kretschmann and H. Raether, Z. Naturforsch. A **23a**, 2135 (1968).

[48] E. Kretschmann, Z. Phys. **241**, 313 (1971).

[49] B. Jusserand and J. Sapriel, Phys. Rev. B **24**, 7194 (1981).